

Passive Stability and Control of Quadrupedal Bounding with a Flexible Torso

Qu Cao and Ioannis Poulakakis

Abstract—This paper studies the stability and control of passively generated bounding motions for a class of quadrupedal template models that incorporate compliant elements in their segmented torso and legs. First, the existence of *self-stable* cyclic bounding gaits in the presence of torso flexibility is examined. Based on numerical studies of the associated Poincaré return map in a dimensionless context, it is deduced that self-stable bounding gaits can indeed be generated through appropriate combinations of the stiffness of the torso and the stiffness of the legs. Next, the implications of this result to control design are discussed, and a hybrid controller is proposed that enhances the stability of the passively generated bounding gaits.

I. INTRODUCTION

A diverse set of robotic quadrupeds has been proposed in the past as part of an effort to realize the potential of legged systems in real-world applications. Examples of robots in this vein include Raibert's quadrupedal machines [1], Scout II [2], Tekken [3], HyQ [4], and BigDog [5], which recently exhibited impressive outdoor mobility. These robots employ a variety of actuation and control schemes and they all involve rigid, non-deformable torsos.

By way of contrast, animals owe much of their remarkable locomotion abilities to their flexible bodies. In fact, research in the context of biomechanics indicates that torso flexibility may improve locomotion performance in a number of ways. Early studies in [6] describe how sagittal-plane oscillations can increase traveling speed by allowing for more ground to be covered per stride. Moreover, elastic structures located in the torso can recycle part of the kinetic energy required to place the legs in high-speed asymmetric running gaits, thereby reducing the cost of transport [7]. Finally, torso bending motions may enhance gait stability through leg angle and angular velocity adjustments prior to touchdown [8].

Quadrupedal robots specifically designed to run by exploiting the benefits of an articulated torso first appeared in the mid-90s with the work of Leeser [9]. Contemporary examples include Canid [10], and the MIT Cheetah quadruped [11], which are currently in the process of development. Recently, Boston Dynamics released a video of their hydraulically actuated Cheetah robot galloping at the record speed of 29 mph [12], demonstrating the potential of realizing fast quadrupedal running motions through a segmented torso. However—to the best of the authors' knowledge—only

limited information on how torso bending movements affect locomotion is available in the context of these platforms.

To investigate the influence of spinal flexion and extension on quadrupedal running, models of varying complexity and different actuation schemes have been proposed. Early work in [13] introduced a sagittal-plane quadrupedal model with a passive flexible torso joint and massless springy legs. However, the difficulty associated with generating periodic motions in the context of this passive model lead to the conclusion that torso flexibility without actuation may render the realization of running motions overly complex. Subsequent efforts in [14] and [15] focused on bounding motions in the presence of an actuated torso spinal joint using a sagittal-plane model with compliant legs. In [14] bounding was generated via PID control loops imposing desired values on the relative angle between the two segments of the torso. On the other hand, in [15] open-loop bounding motions were computed by optimizing actuation profiles. A quasi-passive model was introduced in [16], in which bounding was achieved by assuming that the torso joint can be “locked” when it reaches its maximum flexion and extension.

Motivated by the predictive ability of reduced-order locomotion models like the Spring Loaded Inverted Pendulum (SLIP) [17], [18], the work in [19] investigated the possibility of generating bounding motions without actuation, albeit on a model with a particular geometry and under conditions of reduced gravity. The model introduced in [20] is similar to the one in [19], but the analysis focuses on the stance phase dynamics without considering cyclic motions. Our recent work in [21] examined the conditions under which cyclic bounding can be produced naturally, as the response of the system to suitable initial conditions. Contrary to earlier findings in [13], we have found that such passively generated bounding motions exist, despite the presence of a flexible torso. However, no self-stable motions have been computed in [21]. Very recently, [22] provided preliminary results toward the control of bounding with a passive flexible spine.

In the present paper, we turn our attention to the existence of self-stable bounding motions in the presence of torso flexibility and their implications to controller design. First, we formulate the model proposed in [21] in a non-dimensional setting that facilitates the exploration of the space of possible running solutions. Surprisingly, despite the sensitive dependence of the motion on the torso's dorsoventral oscillations, a number of self-stable periodic bounding motions can be computed through the numerical construction of the associated Poincaré return map. These self-stable bounding motions emerge as a consequence of suitable combinations

This work is supported in part by NSF grant CMMI-1130372 and ARO contract W911NF-12-1-0117.

A video of the results of Section IV accompanies the paper.

Q. Cao and I. Poulakakis are with the Department of Mechanical Engineering, University of Delaware, Newark, DE 19716, USA; e-mail: {caoqu, poulakakis}@udel.edu.

of the torso and leg stiffness parameters. The design of controllers that enlarge the domain of attraction of these self-stable periodic gaits is discussed next, and a hybrid control law acting in both continuous and discrete time is proposed. While the proposed controller uses only a *single* actuator located at the torso joint to stabilize the proposed four-degree-of-freedom (DOF) compliant bounding model, it is capable of rejecting significantly large disturbances without excessive effort.

The structure of the paper is as follows. Section II develops a non-dimensional planar model suitable for studying bounding motions. Section III describes the procedure used to search for passively stable bounding motions, and the relation between the leg and torso stiffness that produces such motions. Section IV proposes a hybrid control law that enlarges the domain of attraction of the self-stable bounding motions of Section III. Section V concludes the paper.

II. A NON-DIMENSIONAL PLANAR BOUNDING MODEL

To incorporate sagittal-plane torso bending motions, the planar model of Fig. 1 was introduced in [21]. The torso consists of two identical rigid bodies connected through a rotational spring intended to introduce flexibility. The posterior (back) and anterior (front) virtual legs represent the collective effect of the posterior and anterior physical leg pairs, and are assumed to be massless prismatic springs. In this work, we restrict our attention to the bounding gait of Fig. 2 which, based on the states of the legs, includes the following phases: double flight, denoted by “f”, in which both legs are in the air in an extended or gathered configuration; the stance-posterior phase, denoted by “sp”, in which the posterior leg is in contact with the ground; and the stance-anterior phase, denoted by “sa”, in which the anterior leg is on the ground.

A. Continuous-time Dynamics in Non-dimensional Form

To derive the dynamics of the model of Fig. 1 we assume that both segments of the torso have mass m and moment of inertia J about their center of mass (COM), and that the hip-to-COM distance is L . The stiffness of the rotational spring connecting the two parts of the torso is denoted by k_{torso} and the stiffness of the virtual legs by k_{leg} . The contact of the legs with the ground is modeled as an unactuated, frictionless pin joint. Through the method of Lagrange, the equations of motion can be written in state-space form as

$$\dot{x}_i = f_i(x_i), \quad (1)$$

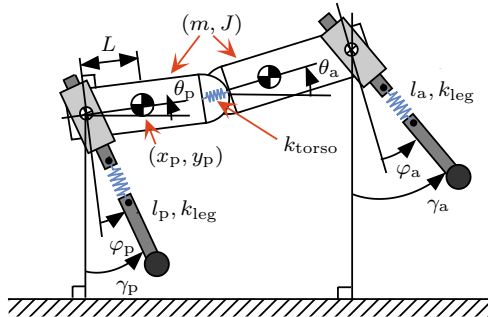


Fig. 1. A sagittal-plane bounding model with a segmented torso.

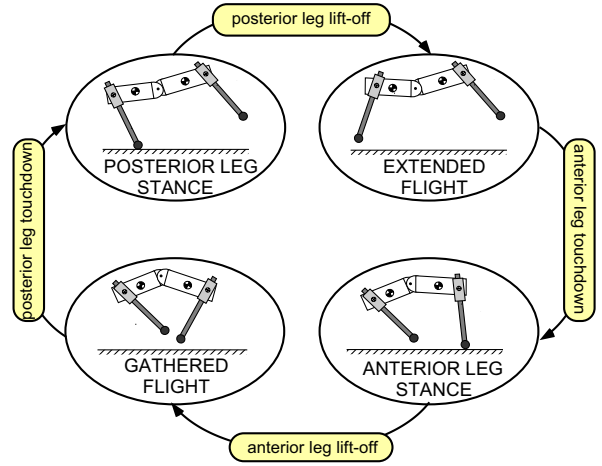


Fig. 2. Bounding phases and events.

evolving in $TQ_i := \{x_i := (q'_i, \dot{q}'_i)' \mid q_i \in Q_i, \dot{q}_i \in \mathbb{R}^4\}$ for $i \in \{f, \text{sp}, \text{sa}\}$. The configuration space Q_f of the extended and gathered flight phases is parameterized through the cartesian coordinates $(x_p, y_p) \in \mathbb{R}^2$ of the COM of the posterior part of the torso, its pitch angle $\theta_p \in \mathbb{S}^1$, and the pitch angle $\theta_a \in \mathbb{S}^1$ of the anterior part of the torso, i.e.,

$$q_f = (x_p, y_p, \theta_p, \theta_a)'. \quad (2)$$

The configuration spaces Q_i , $i \in \{\text{sp}, \text{sa}\}$, of the posterior and anterior leg stance phases are parameterized by the length $l_i \in \mathbb{R}$ of the leg in contact with the ground and its relative angle $\varphi_i \in \mathbb{S}^1$ with respect to the torso, together with the pitch angles $\theta_p \in \mathbb{S}^1$ and $\theta_a \in \mathbb{S}^1$, i.e.,

$$q_i = \begin{cases} (l_p, \varphi_p, \theta_p, \theta_a)' & i = \text{sp}, \\ (l_a, \varphi_a, \theta_p, \theta_a)' & i = \text{sa}. \end{cases} \quad (3)$$

It is important to note that the equations of motion depend on the following six physical parameters

$$\{m, J, l_0, L, k_{\text{torso}}, k_{\text{leg}}\}, \quad (4)$$

which capture the effects of the geometry and the inertia and stiffness properties of the system. In (4), l_0 is the natural length of the legs corresponding to an uncompressed spring; the rest of the parameters have been defined above.

Next, we apply dimensional analysis to transform the dynamics of the system in non-dimensional form. In this form, the parameters (4) that characterize the solutions of (1) reduce to a smaller number of dimensionless quantities, allowing us to explore efficiently a large fraction of the solution space. This will be crucial in computing self-stable bounding motions as will be seen in Section III below.

By defining the characteristic time scale τ as

$$\tau := \sqrt{\frac{l_0}{g}}, \quad (5)$$

where g is the gravitational acceleration, the configuration variables in (1) and their time derivatives obtain the form

$$x_p^* := x_p/l_0, \quad \dot{x}_p^* := \tau \dot{x}_p/l_0, \quad \ddot{x}_p^* := \tau^2 \ddot{x}_p/l_0, \quad (6)$$

$$y_p^* := y_p/l_0, \quad \dot{y}_p^* := \tau \dot{y}_p/l_0, \quad \ddot{y}_p^* := \tau^2 \ddot{y}_p/l_0, \quad (7)$$

$$l_{a,p}^* := l_{a,p}/l_0, \quad \dot{l}_{a,p}^* := \tau \dot{l}_{a,p}/l_0, \quad \ddot{l}_{a,p}^* := \tau^2 \ddot{l}_{a,p}/l_0, \quad (8)$$

$$\varphi_{a,p}^* := \varphi_{a,p}, \quad \dot{\varphi}_{a,p}^* := \tau \dot{\varphi}_{a,p}, \quad \ddot{\varphi}_{a,p}^* := \tau^2 \ddot{\varphi}_{a,p}, \quad (9)$$

$$\theta_{a,p}^* := \theta_{a,p}, \quad \dot{\theta}_{a,p}^* := \tau \dot{\theta}_{a,p}, \quad \ddot{\theta}_{a,p}^* := \tau^2 \ddot{\theta}_{a,p}, \quad (10)$$

where the superscript “*” denotes a dimensionless quantity. Substitution of (6)–(10) to (1) for $i \in \{f, \text{sp}, \text{sa}\}$ reduces the six parameters in (4) to the following four dimensionless parameter groups.

- Relative moment of inertia:

$$I := \frac{J}{mL^2}. \quad (11)$$

- Relative hip-to-COM distance:

$$d := \frac{L}{l_0}. \quad (12)$$

- Relative leg stiffness:

$$\kappa_{\text{leg}} := \frac{k_{\text{leg}} l_0}{mg}. \quad (13)$$

- Relative torso stiffness:

$$\kappa_{\text{torso}} := \frac{k_{\text{torso}}}{mgl_0}. \quad (14)$$

B. Event-based Transitions in Non-dimensional Form

Transitions from one phase to the next follow Fig. 2, and are modeled through suitable threshold functions that describe the conditions for leg touchdown and liftoff. Details can be found in [21, Section II-B]; here we provide the corresponding equations in non-dimensional form.

1) *Flight-to-stance Transitions*: Switching from flight to stance-posterior occurs when the posterior leg touches the ground. This condition is captured by the zeroing of the threshold function

$$H_{f \rightarrow \text{sp}}(x_f^*, \gamma_p^{\text{td}*}) = y_p^* - d \sin \theta_p^* - \cos \gamma_p^{\text{td}*}. \quad (15)$$

Similarly, switching from flight to stance-anterior is given by

$$H_{f \rightarrow \text{sa}}(x_f^*, \gamma_a^{\text{td}*}) = y_p^* + d \sin \theta_p^* + 2d \sin \theta_a^* - \cos \gamma_a^{\text{td}*}, \quad (16)$$

at its zero crossing. In (15) and (16), $\gamma_p^{\text{td}*}$ and $\gamma_a^{\text{td}*}$ are absolute angles of the legs with respect to the vertical prior to touchdown, respectively; see Fig. 1.

2) *Stance-to-flight Transitions*: Switching from stance-anterior and stance-posterior to flight occurs when the corresponding stance leg obtains its natural length. In non-dimensional form the conditions can be captured by the zero crossing of

$$H_{\text{sa} \rightarrow f}(x_{\text{sa}}^*) = l_a^* - 1, \quad \dot{l}_a^* > 0 \quad (17)$$

and

$$H_{\text{sp} \rightarrow f}(x_{\text{sp}}^*) = l_p^* - 1, \quad \dot{l}_p^* > 0, \quad (18)$$

respectively.

C. Hybrid Dynamics of Bounding in Non-dimensional Form

To examine the existence and local stability properties of the bounding motions according to the phase sequence of Fig. 2, we use Poincaré’s method. The Poincaré section is taken at the apex height of the torso joint in the extended flight, where its vertical velocity becomes zero; i.e.

$$\mathcal{S}_{\text{apex}}^* := \left\{ x_f^* \in TQ_f^* \mid \dot{y}_p^* + d\dot{\theta}_p^* \cos \theta_p^* = 0, \quad \theta_a^* > 0 \right\}, \quad (19)$$

where TQ_f^* is the flight phase state space parameterized by the non-dimensional variables defined previously. Discarding the horizontal distance x_p^* travelled by the posterior part of the torso, which is monotonically increasing and cannot map to itself after one cycle, the (reduced) Poincaré map $\mathcal{P}^* : \mathcal{S}_{\text{apex}}^* \rightarrow \mathcal{S}_{\text{apex}}^*$ can be defined as

$$z_f^*[k+1] = \mathcal{P}^*(z_f^*[k], \alpha_f^*[k]), \quad (20)$$

where $z_f^* := (y_p^*, \theta_p^*, \theta_a^*, \dot{x}_p^*, \dot{\theta}_p^*, \dot{\theta}_a^*)'$ and α_f^* contains the absolute touchdown angles, i.e., $\alpha_f^* := (\gamma_a^{\text{td}*}, \gamma_p^{\text{td}*})'$.

III. SELF-STABLE BOUNDING MOTIONS

This section uses the planar model of Fig. 1 in the non-dimensional context of Section II to demonstrate that passively stable bounding motions are possible in the presence of a flexible torso without the need of actuation.

A. Passively Generated Fixed Points

Computing a fixed point for (20) is equivalent to finding an argument z_f^* in (20) that maps onto itself

$$z_f^* - \mathcal{P}^*(z_f^*, \alpha_f^*) = 0, \quad (21)$$

for physically reasonable values of touchdown angles α_f^* .

The equation (21) is solved numerically using MATLAB’s `fsolve` and a large number of bounding gaits have been computed by supplying the system with suitable initial conditions and touchdown angles. Their properties will not be discussed here; see [21] for details. We only mention the fact that the system possesses a time-reversing symmetry; this fact allows us to restrict our attention to fixed points at which the pitch angles of the two segments of the torso obey the relations

$$\theta_a^* = -\theta_p^* \quad \text{and} \quad \dot{\theta}_a^* = \dot{\theta}_p^*, \quad (22)$$

at the apex of the flight phases. These relations will be used in the present paper to reduce the number of variables involved in the search for passively stable fixed points.

B. Passively Stable Fixed Points

To analyze the local stability properties of bounding, we linearize (20) at a fixed point $(\bar{z}_f^*, \bar{\alpha}_f^*)$ resulting in

$$\Delta z_f^*[k+1] = A \Delta z_f^*[k] + B \Delta \alpha_f^*[k], \quad (23)$$

where $\Delta z_f^* = z_f^* - \bar{z}_f^*$, and $\Delta \alpha_f^* = \alpha_f^* - \bar{\alpha}_f^*$, and

$$A = \left. \frac{\partial \mathcal{P}^*}{\partial z_f^*} \right|_{z_f^* = \bar{z}_f^*, \alpha_f^* = \bar{\alpha}_f^*}, \quad B = \left. \frac{\partial \mathcal{P}^*}{\partial \alpha_f^*} \right|_{z_f^* = \bar{z}_f^*, \alpha_f^* = \bar{\alpha}_f^*}. \quad (24)$$

Due to the energy conservative nature, ones of the eigenvalues of matrix A is always one. Thus, when the remaining

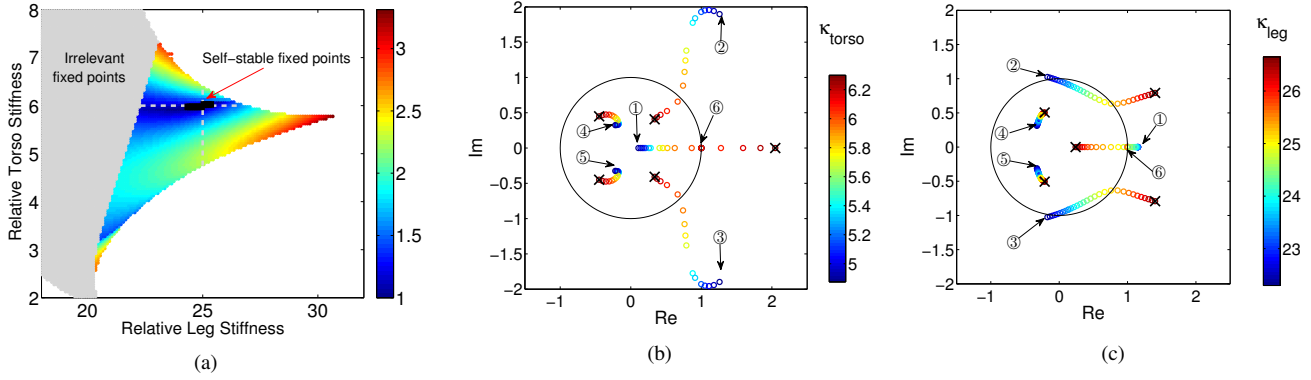


Fig. 3. (a) Fixed points computed for the same dimensionless total energy (7.95), average speed (2.41) and hopping height (0.818) and for different values of dimensionless leg and torso stiffness. The color code corresponds to the values of the spectral radius of matrix A . (b) The paths of the six eigenvalues for $\kappa_{\text{leg}} = 25$ and $\kappa_{\text{torso}} \in [4.88, 6.30]$ corresponding to the vertical grey dotted line in (a). (c) The paths of the six eigenvalues for $\kappa_{\text{torso}} = 6.00$ and $\kappa_{\text{leg}} \in [22.30, 26.65]$ corresponding to the horizontal grey dotted line in (a).

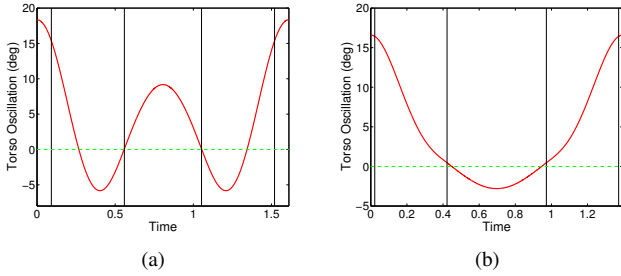


Fig. 4. Torso flexion-extension oscillation in one stride for two fixed points. (a) A fixed point in the grey area of Fig. 3(a). (b) A physically meaningful fixed point in Fig. 3(a).

eigenvalues are all within the unit disc, the corresponding fixed point is locally exponentially stable within the same energy level.

All the fixed points computed in [21] correspond to specific values of the parameters in (4), and have been found to be unstable. However, the non-dimensional form of the dynamics allows us to explore systematically the space of solutions for various combinations of the dimensionless parameters introduced in Section II. Of particular interest in this work are the combinations of the relative torso and leg stiffness values that generate bounding motions; note, however, that other parameter combinations can also be examined.

Fig. 3(a) shows how the spectral radius $\rho(A) := \max_i |\lambda_i|$ of the matrix A in (23) changes as a function of the pair $(\kappa_{\text{leg}}, \kappa_{\text{torso}})$ keeping the rest of the dimensionless parameters—namely, I and d defined by (11) and (12), respectively—constant. The grey area in Fig. 3(a) corresponds to periodic motions with torso bending movements similar to Fig. 4(a), in which the torso oscillates multiple times within one stride. This type of behavior appears for small values of leg stiffness; clearly, a softer leg requires a longer time period to go through a complete compression and decompression phase during stance, allowing the torso to oscillate as in Fig. 4(a). For reasons of comparison, the torso oscillation corresponding to one of the self-stable fixed points is depicted in Fig. 4(b).

An interesting observation from Fig. 3(a) is that the range

of values of the relative leg stiffness over which bounding gaits—not necessarily stable ones—can be generated passively depends strongly on the combination of relative torso and leg stiffness. For example, when $\kappa_{\text{torso}} = 3.6$ passively generated bounding orbits exist for $\kappa_{\text{leg}} \in [20.80, 21.55]$. On the other hand, when $\kappa_{\text{torso}} = 5.4$, bounding orbits can be generated for $\kappa_{\text{leg}} \in [22.00, 28.15]$, a significantly wider region than that corresponding to $\kappa_{\text{torso}} = 3.6$. This observation shows the sensitive dependence of the system’s behavior on the combination between the stiffness of the torso and the stiffness of the legs.

Fig. 3(a) also illustrates that self-stable bounding motions emerge for particular combinations of the relative torso and leg stiffness. However, these motions correspond to a small fraction of the bounding gaits that can be generated passively. This can be explained by Figs. 3(b) and 3(c) that show the loci of the eigenvalues of A in (23) as the parameters κ_{torso} and κ_{leg} vary. In interpreting Figs. 3(b) and 3(c) note that the numbers show the points at which the eigenvalues start and “x” the points at which they terminate. In all cases, one of the eigenvalues—namely, the eigenvalue denoted by “6”—remains at one, due to the conservative nature of the system. In more detail, Fig. 3(b) indicates that as the torso stiffness κ_{torso} increases for a given value of κ_{leg} the eigenvalues “2” and “3” enter the unit circle. However, the eigenvalue “1” eventually exits from the unit circle, implying an upper bound on κ_{torso} exists, beyond which instability occurs. On the other hand, Fig. 3(c) shows that keeping κ_{torso} constant and increasing κ_{leg} moves the eigenvalue “1” inside the unit circle, but the eigenvalues “2” and “3” exhibit the opposite behavior: while they initially enter the unit circle, they eventually move outside of it. In both cases, the range of parameter values that correspond to self-stable motions is narrow, explaining the difficulty in computing such motions in our previous work [21], and in other efforts [13], [16].

As a final remark, note that the emergence of self-stability in the presence of a flexible segmented torso should not be considered as an immediate consequence of the existence of self-stable bounding orbits in the context of quadrupedal models with rigid torso [2], [23]. The reason is that torso

bending movements may cause divergent behavior when they are not properly coordinated with the hybrid oscillations of the legs. As noted in [2], [23] for the rigid-torso case, the inertia properties of the torso—captured by the dimensionless moment of inertia of the torso—dominate self-stability. On the other hand, in the flexible-torso case, the combination of the stiffness properties of the legs and the torso is the dominant factor for stability.

IV. FEEDBACK CONTROL

The existence of passively generated bounding orbits and its relation to key design parameters that couple the stiffness, inertia and geometric properties of the model can provide useful information regarding the design of quadrupedal robots with a flexible torso. In terms of stability, however, it is clear that the model in its current passive and conservative form cannot reject disturbances that perturb the total energy of the system. Furthermore, even when the applied perturbations do not alter the total energy level, the domain of attraction of the self-stable bounding orbits found in Section III-B is not sufficiently large to ensure convergence. Clearly, the development of control laws is necessary to sustain periodic bounding orbits in the presence of perturbations. This section takes a step toward this direction by proposing a controller that uses a *single* actuator to enhance the stability of the 4-DOF compliant bounding model discussed so far.

To enable the development of non-conservative corrective forces, the model is modified to include one actuator in parallel with the torso spring. With this modification, the open-loop dynamics of the system in each phase $i \in \{f, sp, sa\}$ becomes

$$\dot{x}_i = f_i(x_i) + g_i(x_i)u_i, \quad (25)$$

where u_i is the input torque. For concreteness, we consider a model with mechanical properties that roughly correspond to the quadrupedal robot Scout II [2]; see Table I.

TABLE I
MECHANICAL PARAMETERS OF THE MODEL

Parameter	Value	Units
Torso Mass (m)	10.432	kg
Torso Inertia (J)	0.36	kg m ²
Hip-to-COM spacing (L)	0.138	m
Nominal Leg Length (l_0)	0.36	m
Leg Spring Constant (k_{leg})	7329	N/m
Torso Spring Constant (k_{torso})	203	Nm/rad

In general terms, the structure of the proposed controller exploits the hybrid nature of the system by introducing control action on two levels. On the first level, a continuous-time controller is employed at the torso joint to impose a virtual (holonomic) constraint that coordinates the torso and legs according to a passively generated bounding orbit of Section III-B; the orbit is selected to satisfy desired forward velocity and hopping height specifications. On the second level, a discrete-time controller that uses event-based feedback of the forward velocity is engaged to update the leg touchdown angles.

It should be mentioned here that in rigid-torso models, the stability of the torso pitch oscillation in bounding emerges without direct control over the pitch angle for a wide range of initial conditions [1, Chapter 8]. However, in models with a segmented flexible torso, the additional degree of freedom that corresponds to the torso relative pitch oscillations is very sensitive to perturbations and highly coupled to the leg motion. The controller proposed here restricts the torso relative pitch oscillation according to the leg motion, effectively reducing the system so that the stability of its motion can be enhanced through leg touchdown angle updates in an event-based fashion.

1) *Continuous-time Control*: For each phase $i \in \{sp, sa, f\}$ we associate to the continuous dynamics (25) the output function

$$y_i = h_i(q_i) := H_i q_i - h_{P,i}^d(q_i), \quad (26)$$

where $H_i := [0 \ 0 \ -1 \ 1]$ so that, by (2) and (3), the controlled variable $H_i q_i$ corresponds to the relative pitch angle $\theta_a - \theta_p$ and $h_{P,i}^d(q_i)$ is its desired evolution. Note that in (26), $h_i(q_i)$ is a function of the configuration variables (not time), and therefore it can be interpreted as a (virtual) holonomic constraint, which can be imposed via a control law whose objective is to drive the output to zero. To simplify¹ the development, PD control laws will be employed to achieve this objective; i.e.,

$$u_i = K_{P,i} y_i + K_{D,i} \dot{y}_i, \quad (27)$$

where $K_{P,i}$ and $K_{D,i}$ are selected gains.

It is through the design of $h_{P,i}^d(q_i)$ in (26) that information about the leg-torso coordination pattern that characterizes the selected passively generated gait is passed to the controller. In more detail, $h_{P,i}^d(q_i)$ is designed through a suitable parameterization of the evolution of the relative pitch angle $\theta_a - \theta_p$ at the selected (desired) passive gait. To simplify the implementation, for $i \in \{f, sp, sa\}$, $h_{P,i}^d(q_i)$ is selected as a fifth degree polynomial

$$h_{P,i}^d(q_i) = \sum_{k=0}^5 a_{i,k} s^k(q_i), \quad (28)$$

fitted to the nominal (according to the desired passive orbit) evolution of $\theta_a - \theta_p$. It is important to note that s is *not* an

¹Feedback linearization techniques as in [24] can also be used.

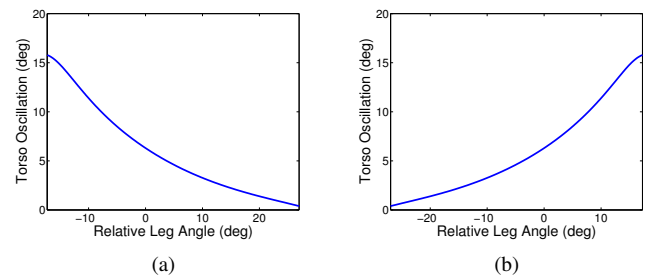


Fig. 5. The relative torso pitch angle $\theta_a - \theta_p$ as a function of the leg angle φ_p and φ_a in the posterior (a), and the anterior (b) stance. The monotonic relation allows to coordinate the torso oscillation with the leg sweeping motion through a virtual holonomic constraint.

explicit function of time. Utilizing the fact that during the stance phases, $\theta_a - \theta_p$ is a (strictly) monotonic function of the angle of the stance leg relative to the torso—see also Fig. 5—the function $s(q_i)$, $i \in \{\text{sp}, \text{sa}\}$ can be selected as

$$s(q_i) := \frac{\bar{\varphi}^{\max} - \varphi}{\bar{\varphi}^{\max} - \bar{\varphi}^{\min}}, \quad (29)$$

where $\varphi = \varphi_p$ for $i = \text{sp}$ and $\varphi = \varphi_a$ for $i = \text{sa}$, and $\bar{\varphi}^{\min}$ and $\bar{\varphi}^{\max}$ are the minimum and maximum values of φ in the corresponding stance phase during the nominal motion. Intuitively, with this parametrization, the virtual constraint design (26) ensures that the torso extends during the posterior stance phase and it flexes during the subsequent anterior stance phase, and that this flexion-extension oscillation is coordinated with the nominal motion through the sweeping angle of the corresponding stance leg.

In a similar fashion, during flight $s(q_f)$ is computed as

$$s(q_i) := \frac{x_{\text{tj}}(q_i) - \bar{x}_{\text{tj}}^{\min}}{\bar{x}_{\text{tj}}^{\max} - \bar{x}_{\text{tj}}^{\min}}, \quad (30)$$

where x_{tj} is the distance travelled by the torso joint,

$$x_{\text{tj}}(q_i) := x_p + L \cos \theta_p, \quad (31)$$

and $\bar{x}_{\text{tj}}^{\min}$ and $\bar{x}_{\text{tj}}^{\max}$ are its values at the beginning and at the end of the flight phase, respectively.

Note that when the system in closed-loop with the continuous-time controlled described above bounds along a nominal orbit, the torques developed by the actuator are very small, but are not exactly equal to zero; see also Section IV-3 below. This is due to the numerical errors introduced by the fitting process. Increasing the degree of the polynomials in (28) can decrease the fitting error. To further suppress the residual torques after convergence to the nominal gait, the PD controller (27) can be implemented using

$$\dot{y}_i = H_i \dot{q}_i - h_{V,i}^d(q_i), \quad (32)$$

where, instead of differentiating (28) with respect to time, $h_{V,i}^d(q_i)$ is obtained by fitting a new polynomial to the rate of change of y_i . This idea has been employed in [24] in the context of passive bipedal walking, and is very effective in reducing the torques that are present in the nominal motion.

2) *Discrete-time Control*: The discrete-time controller simply updates the touchdown angles of the anterior and posterior legs at the apex of the gathered flight based on feedback of the horizontal velocity of the torso spinal joint,

$$\gamma_i^{\text{td}}[k] = \bar{\gamma}_i^{\text{td}} + K_i(x_{\text{tj}}[k] - \bar{x}_{\text{tj}}), \quad (33)$$

where $i \in \{\text{a}, \text{p}\}$ and $\bar{\cdot}$ denotes the nominal value.

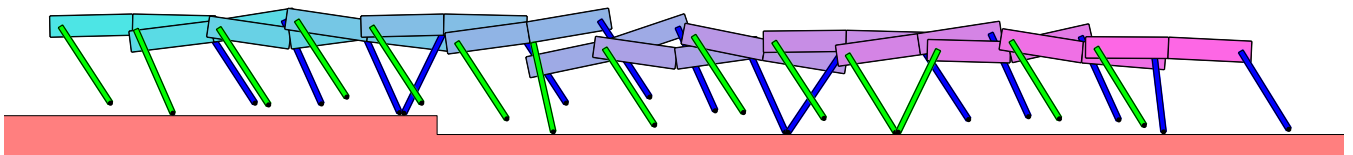


Fig. 6. Snapshots of the model's motion as it runs down a step of 7.2cm (20% of the nominal leg length).

3) *Simulation Results*: To test the controller, we examined the response of the system when encountering an unexpected variation in the ground height that is equal to 20% of the nominal leg length. Fig. 6 shows snapshots of the system's motion as it converges to a periodic orbit, which corresponds to the nominal one when the hopping height is measured from the new ground level; see also the video accompanying this submission.

Fig. 7 shows convergence to the nominal values of the hopping height, forward velocity and the total energy of the system. Fig. 8(a) shows the corresponding input torque developed by the torso joint actuator for the first four strides. During the first stride which is along the nominal orbit, the torque is close, but not exactly equal to zero due to the fitting errors associated with (28). In the recovering strides, the size of the input torque remains within practically reasonable bounds due to the existence of the torso spring, and eventually becomes very small when the system converges to its nominal motion. The corresponding ground reaction forces are shown in Fig. 8(b); their profile is similar to the one used to generate bounding through force planning in [25]. After the step-down disturbance, the magnitudes of both vertical and horizontal components increase due to the fact that part of the gravitational potential energy is transferred to the leg spring resulting in larger compression. Note that the friction cone limitations are respected throughout the motion.

Finally, it is remarked that the proposed control law is capable of stabilizing a 4-DOF compliant system undergoing significantly large disturbances with only one actuator. Additional actuators can be included at the hips and/or the legs to further improve the performance of the controller or to achieve additional objectives in more complete higher-dimensional robot models. The results in the present paper should be considered as a first step toward this direction.

V. CONCLUSIONS

In this paper, the existence and stability of passively generated bounding running gaits were studied in the context of a reductive sagittal-plane model with a flexible segmented torso and compliant legs. Based on the analysis of the corresponding Poincaré return map in a non-dimensional form, it was found that stable bounding could be passively generated for certain combinations of physical parameters and appropriate initial conditions. The relationship between the leg and torso spring stiffness was discussed, quantifying the sensitive dependence of the torso flexion and extension oscillations on the movement of the legs. Finally, to enhance stability, a hybrid feedback controller that takes advantage of the leg-torso coordination corresponding to a passive

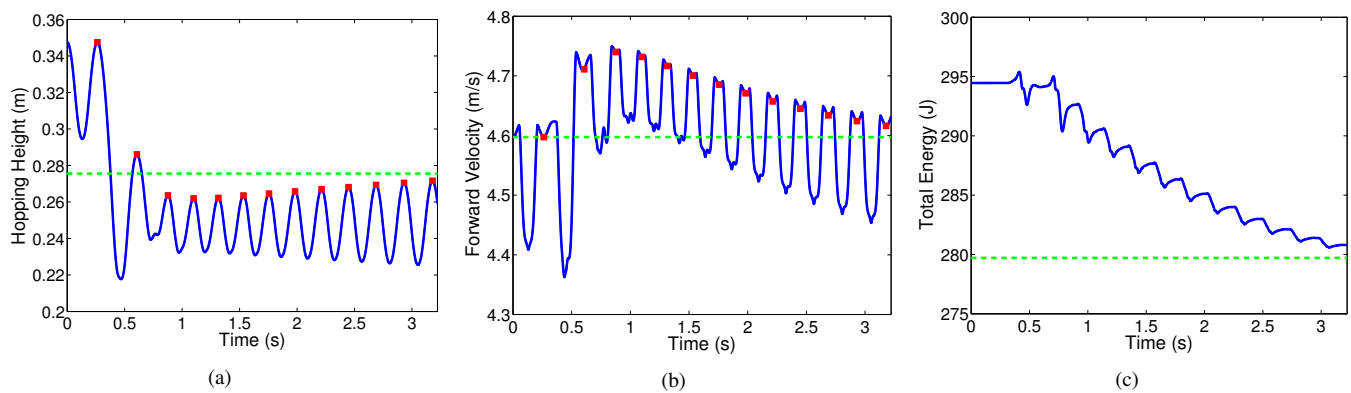


Fig. 7. Response of the system to a step-down disturbance of 7.2cm showing convergence to the nominal orbit. (a) Hopping height; (b) Forward velocity; (c) Total energy. The red squares represent the apex height in the gathered flight and the green dotted lines represent the final values.

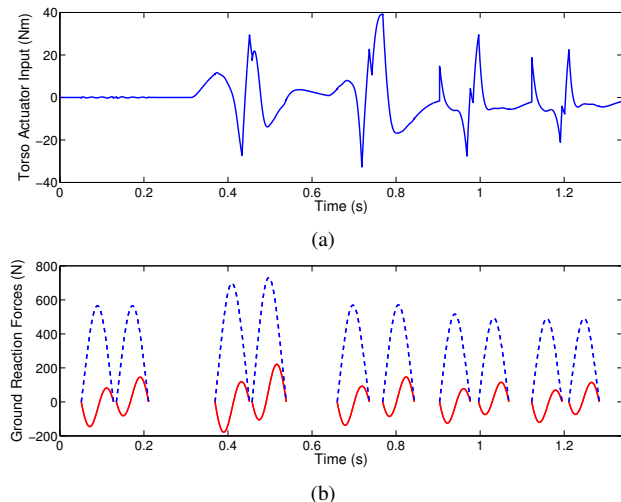


Fig. 8. (a) The input of the torso joint actuator. (b) Horizontal (red continuous) and vertical (blue dotted) components of ground reaction force. For clarity, only five strides are presented.

gait was proposed. The controller was capable of rejecting significantly large disturbances with only a single actuator.

REFERENCES

- [1] M. H. Raibert, *Legged Robots that Balance*. Cambridge, MA: MIT Press, 1986.
- [2] I. Poulakakis, E. G. Papadopoulos, and M. Buehler, "On the stability of the passive dynamics of quadrupedal running with a bounding gait," *The International Journal of Robotics Research*, vol. 25, no. 7, pp. 669–687, 2006.
- [3] Y. Fukuoka, H. Kimura, and A. H. Cohen, "Adaptive dynamic walking of a quadruped robot on irregular terrain based on biological concepts," *The International Journal of Robotics Research*, vol. 23, no. 10–11, pp. 1059–1073, 2004.
- [4] C. Semini, N. G. Tsagarakis, E. Guglielmino, M. Focchi, F. Cannella, and D. G. Caldwell, "Design of HyQ - a hydraulically and electrically actuated quadruped robot," *Proceedings of the IMechE Part I: Journal Systems and Control Engineering*, vol. 225, no. 6, pp. 831–849, 2011.
- [5] M. Raibert, K. Blankespoor, G. Nelson, R. Playter, and the BigDog Team, "BigDog, the rough-terrain quadruped robot," in *Proceedings of the 17th IFAC World Congress*, Seoul, Korea, July 2008, pp. 10 822–10 825.
- [6] M. Hildebrand, "Motions of the running cheetah and horse," *Journal of Mammalogy*, vol. 40, no. 4, pp. 481–495, 1959.
- [7] R. Alexander, N. J. Dimery, and R. F. Ker, "Elastic structures in the back and their role in galloping in some mammals," *Journal of Zoology A*, vol. 207, pp. 467–482, 1985.
- [8] N. Schilling and R. Hackert, "Sagittal spine movements of small therian mammals during asymmetrical gaits," *Journal of Experimental Biology*, vol. 209, pp. 3925–3939, 2006.
- [9] K. F. Leiser, "Locomotion experiments on a planar quadruped robot with articulated spine," Master's thesis, Massachusetts Institute of Technology, February 1996.
- [10] G. C. Haynes, J. Pusey, R. Knopf, A. M. Johnson, and D. E. Koditschek, "Laboratory on legs: An architecture for adjustable morphology with legged robots," in *Proceedings of the SPIE Defense, Security, and Sensing Conference, Unmanned Systems Technology XIV (8387)*, 2012.
- [11] S. Kim. (2013) Cheetah-inspired quadruped. Mar. 15, 2013. [Online]. Available: <http://biomimetics.mit.edu:8100/wordpress/>
- [12] Boston Dynamics. (2012) CHEETAH - fastest legged robot. Mar. 15, 2013. [Online]. Available: <http://www.bostondynamics.com/>
- [13] P. Nanua, "Dynamics of a galloping quadruped," Ph.D. dissertation, Ohio State University, 1992.
- [14] U. Culha and U. Saranlı, "Quadrupedal bounding with an actuated spinal joint," in *Proceedings of the IEEE International Conference on Robotics and Automation*, 2011, pp. 1392–1397.
- [15] S. Pouya, M. Khodabakhsh, R. Moeckel, and A. J. Ijspeert, "Role of spine compliance and actuation in the bounding performance of quadruped robots," in *Proceedings of the Dynamic Walking Conference*, 2012.
- [16] Q. Deng, S. Wang, W. Xu, J. Mo, and Q. Liang, "Quasi passive bounding of a quadruped model with articulated spine," *Mechanism and Machine Theory*, vol. 52, pp. 232–242, 2012.
- [17] R. Full and D. E. Koditschek, "Templates and anchors: Neuromechanical hypotheses of legged locomotion on land," *Journal of Experimental Biology*, vol. 202, pp. 3325–3332, 1999.
- [18] I. Poulakakis and J. W. Grizzle, "Monopodal running control: SLIP embedding and virtual constraint controllers," in *Proceedings of the IEEE/RSJ International Conference of Intelligent Robots and Systems*, San Diego, U.S.A., Oct. 2007, pp. 323–330.
- [19] J. E. Seipel, "Analytic-holistic two-segment model of quadruped back-bending in the sagittal plane," in *ASME Mechanisms and Robotics Conference*, vol. 6, 2011, pp. 855–861.
- [20] G. C. Haynes, J. Pusey, R. Knopf, and D. E. Koditschek, "Dynamic bounding with a passive compliant spine," in *Proceedings of the Dynamic Walking Conference*, 2012.
- [21] Q. Cao and I. Poulakakis, "Passive quadrupedal bounding with a segmented flexible torso," in *Proceedings of the IEEE/RSJ International Conference on Intelligent Robots and Systems*, 2012, pp. 2484–2489.
- [22] B. Satzinger and K. Byl, "Control of planar bounding quadruped with passive flexible spine," in *International Symposium of Adaptive Motion in Animals and Machines*, 2013.
- [23] P. Chatzakos and E. Papadopoulos, "Self-stabilizing quadrupedal running by mechanical design," *Applied Bionics and Biomechanics*, vol. 6, no. 1, pp. 73–85, 2009.
- [24] E. R. Westervelt, B. Morris, and K. D. Farrell, "Analysis results and tools for the control of planar bipedal gaits using hybrid zero dynamics," *Autonomous Robots*, vol. 23, no. 2, pp. 131–145, 2007.
- [25] A. K. Valenzuela and S. Kim, "Optimally scaled hip-force planning: A control approach for quadrupedal running," in *Proceedings of the IEEE International Conference on Robotics and Automation*, 2012, pp. 1901–1907.